8. DIRC

8.1. Purpose and Design Requirements

The study of *CP*-violation requires the ability to tag the flavor of one of the B mesons via the cascade decay $b \to c \to s$, while fully reconstructing the second B decay. The momenta of the kaons used for flavor tagging extend up to about 2 GeV/c, with most of them below 1 GeV/c. On the other hand, pions and kaons from the rare two-body decays $B^0 \to \pi^+\pi^-$ and $B^0 \to K^+\pi^-$ must be well-separated. They have momenta between 1.7 and 4.2 GeV/c with a strong momentum-polar angle correlation of the tracks (higher momenta occur at more forward angles because of the c.m. system boost) [4].

The *Particle Identification* (PID) system should be thin and uniform in terms of radiation lengths (to minimize degradation of the calorimeter energy resolution) and small in the radial dimension to reduce the volume, and hence, the cost of the calorimeter. Finally, for operation at high luminosity, the PID system needs fast signal response, and should be able to tolerate high backgrounds.

The PID system being used in *BABAR* is a new kind of ring-imaging Cherenkov detector called the DIRC [56] (the acronym DIRC stands for *Detector of Internally Reflected Cherenkov* light). It is expected to be able to provide π/K separation of $\sim 4\ \sigma$ or greater, for all tracks from B-meson decays from the pion Cherenkov threshold up to 4.2 GeV/c. PID below 700 MeV/c relies primarily on the dE/dx measurements in the DCH and SVT.

8.2. DIRC Concept

The DIRC is based on the principle that the magnitudes of angles are maintained upon reflection from a flat surface. Figure 48 shows a schematic of the DIRC geometry that illustrates the principles of light production, transport, and imaging. The radiator material of the DIRC is synthetic, fused silica in the form of long, thin bars with rectangular cross section. These bars serve both as radiators and as light pipes for the portion of the light trapped in the radiator by total internal reflection. Fused, synthetic silica

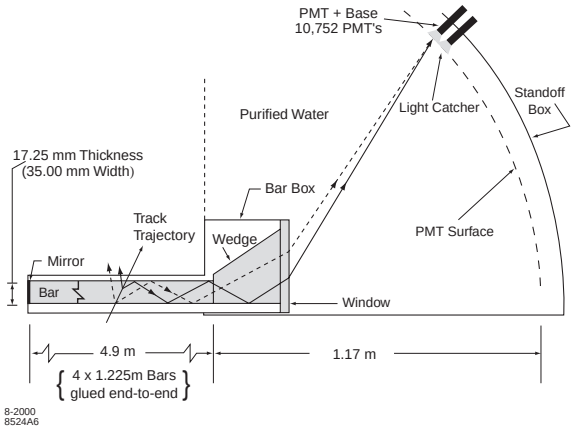

Figure 48. Schematics of the DIRC fused silica radiator bar and imaging region. Not shown is a 6 mrad angle on the bottom surface of the wedge (see text).

(Spectrosil [57]) is chosen because of its resistance to ionizing radiation, its long attenuation length, large index of refraction, low chromatic dispersion within the wavelength acceptance of the DIRC, and because it allows an excellent optical finish on the surfaces of the bars [58].

In the following, the variable θ_c is used to designate the Cherenkov angle, ϕ_c denotes the azimuthal angle of a Cherenkov photon around the track direction, and n represents the mean index of refraction of fused silica ($n = 1.473$), with the familiar relation $\cos\theta_c = 1/n\beta$ ($\beta = v/c$, $v =$ velocity of the particle, $c =$ velocity of light).

For particles with $\beta \approx 1$, some photons will always lie within the total internal reflection limit, and will be transported to either one or both ends of the bar, depending on the particle incident angle. To avoid instrumenting both ends of the bar with photon detectors, a mirror is placed at the forward end, perpendicular to the bar axis, to reflect incident photons to the backward, instrumented end.

Once photons arrive at the instrumented end, most of them emerge into a water-filled expansion region, called the *standoff box*. A fused silica *wedge* at the exit of the bar reflects photons at large angles relative to the bar axis. It thereby

reduces the size of the required detection surface and recovers those photons that would otherwise be lost due to internal reflection at the fused silica/water interface. The photons are detected by an array of densely packed photomultiplier tubes (PMTs), each surrounded by reflecting *light catcher* cones [59] to capture light which would otherwise miss the active area of the PMT. The PMTs are placed at a distance of about 1.2 m from the bar end. The expected Cherenkov light pattern at this surface is essentially a conic section, where the cone opening-angle is the Cherenkov production angle modified by refraction at the exit from the fused silica window.

The DIRC is intrinsically a three-dimensional imaging device, using the position and arrival time of the PMT signals. Photons generated in a bar are focused onto the phototube detection surface via a "pinhole" defined by the exit aperture of the bar. In order to associate the photon signals with a track traversing a bar, the vector pointing from the center of the bar end to the center of each PMT is taken as a measure of the photon propagation angles α_x, α_y, and α_z. Since the track position and angles are known from the tracking system, the three α angles can be used to determine the two Cherenkov angles θ_c and ϕ_c. In addition, the arrival time of the signal provides an independent measurement of the propagation of the photon, and can be related to the propagation angles α. This over-constraint on the angles and the signal timing are particularly useful in dealing with ambiguities in the signal association (see Section 8.6.1) and high background rates.

8.3. Mechanical Design and Physical Description

The DIRC bars are arranged in a 12-sided polygonal barrel. Because of the beam energy asymmetry, particles are produced preferentially forward in the detector. To minimize interference with other detector systems in the forward region, the DIRC photon detector is placed at the backward end.

The principal components of the DIRC are shown schematically in Figure 49. The bars are placed into 12 hermetically sealed containers, called *bar boxes*, made of very thin aluminum-hexcel panels. Each bar box, shown in Figure 50, contains 12 bars, for a total of 144 bars. Within a bar box the 12 bars are optically isolated by a $\sim 150\mu m$ air gap between neighboring bars, enforced by custom shims made from aluminum foil.

The bars are 17 mm-thick, 35 mm-wide, and 4.9 m-long. Each bar is assembled from four 1.225 m pieces that are glued end-to-end; this length is the longest high-quality bar currently obtainable [58, 60].

The bars are supported at 600 mm intervals by small nylon buttons for optical isolation from the bar box. Each bar has a fused silica wedge glued to it at the readout end. The wedge, made of the same material as the bar, is 91 mm-long with very nearly the same width as the bars (33 mm) and a trapezoidal profile (27 mm-high at bar end, and 79 mm at the light exit end). The bottom of the wedge (see Figure 48) has a slight (~ 6 mrad) upward slope to minimize the displacement of the downward reflected image due to the finite bar thickness. The twelve wedges in a bar box are glued to a common 10 mm-thick fused silica window, that provides the interface and seal to the purified water in the standoff box.

The mechanical support of the DIRC, shown in Figure 49, is cantilevered from the steel of the IFR. The *Strong Support Tube* (SST) is a steel cylinder located inside the end doors of the IFR and provides the basic support for the entire DIRC. In turn, the SST is supported by a steel *support gusset* that fixes it to the barrel magnet steel. It also minimizes the magnetic flux gap caused by the DIRC bars extending through the flux return, and supports the axial load of the inner magnetic plug surrounding the beam in this region.

The bar boxes are supported in the active region by an aluminum tube, the *Central Support Tube* (CST), attached to the SST via an aluminum transition flange. The CST is a thin, double-walled, cylindrical shell, using aircraft-type construction with stressed aluminum skins and bulkheads having riveted or glued joints. The CST also provides the support for the DCH.

The standoff box is made of stainless steel, consisting of a cone, cylinder, and 12 sectors of

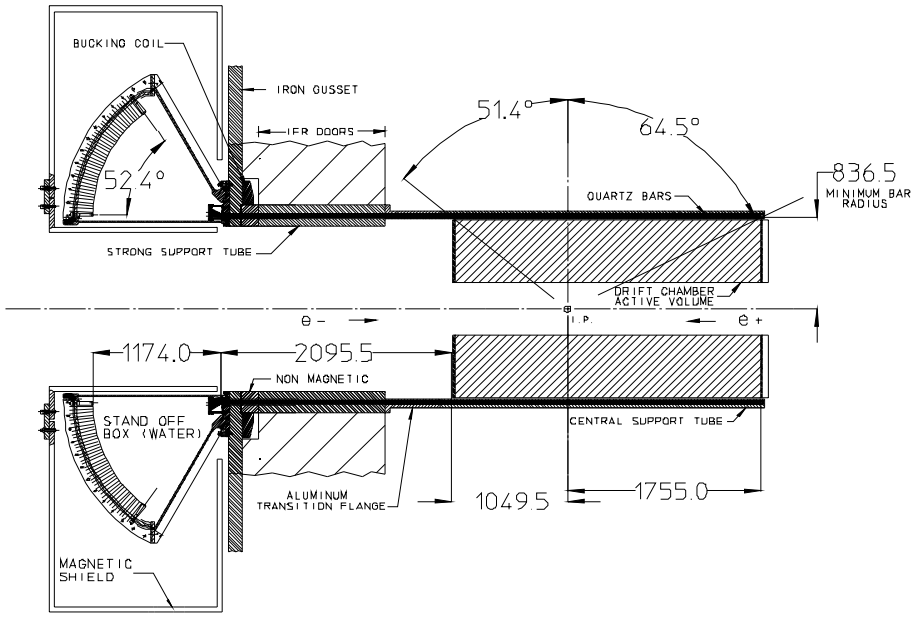

Figure 51. Elevation view of the nominal DIRC system geometry. For clarity, the end plug is not shown. All dimensions are given in mm.

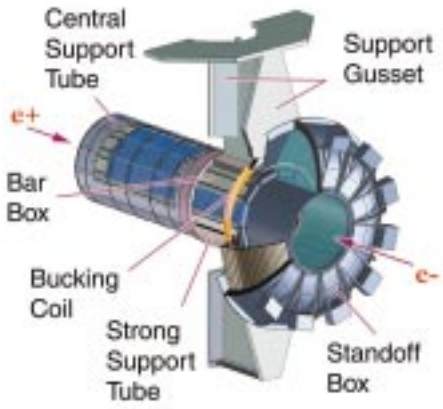

Figure 49. Exploded view of the DIRC mechanical support structure. The steel magnetic shield is not shown.

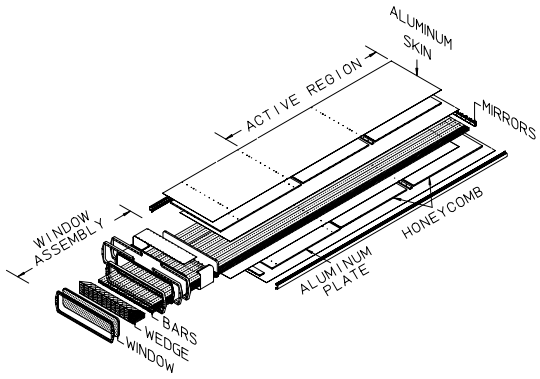

Figure 50. Schematics of the DIRC bar box assembly.

PMTs. It contains about 6,000 liters of purified water. Water is used to fill this region because it is inexpensive and has an average index of refraction ($n \approx 1.346$) reasonably close to that of fused silica, thus minimizing the total internal reflection at silica-water interface. Furthermore, its chromaticity index is a close match to that of fused silica, effectively eliminating dispersion at the silica-water interface. The steel gusset supports the standoff box. A steel shield, supplemented by a *bucking coil*, surrounds the standoff box to reduce the field in the PMT region to below 1 Gauss [28].

The PMTs at the rear of the standoff box lie on a surface that is approximately toroidal. Each

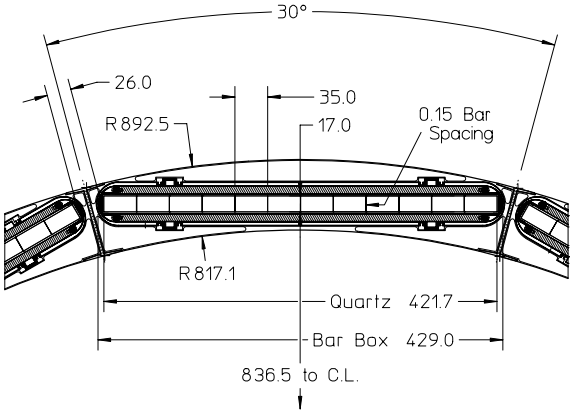

Figure 52. Transverse section of the nominal DIRC bar box imbedded in the CST. All dimensions are given in mm.

of the 12 PMT sectors contains 896 PMTs (ETL model 9125 [61,62]) with 29 mm-diameter, in a closely packed array inside the water volume. A double o-ring water seal is made between the PMTs and the wall of the standoff box. The PMTs are installed from the inside of the standoff box and connected via a feed-through to a base mounted outside. The hexagonal light catcher cone is mounted in front of the photocathode of each PMT, which results in an effective active surface area light collection fraction of about 90%. The geometry of the DIRC is shown in Figures 51 and 52.

The DIRC occupies 80 mm of radial space in the central detector volume including supports and construction tolerances, with a total of about 17% radiation length thickness at normal incidence. The radiator bars subtend a solid angle corresponding to about 94% of the azimuth and 83% of the c.m. polar angle cosine.

The distance from the end of the bar to the PMTs is ~ 1.17 m, which together with the size of the bars and PMTs, gives a geometric contribution to the single photon Cherenkov angle resolution of ~ 7 mrad. This value is slightly larger than the rms spread of the photon production (dominated by a ~ 5.4 mrad chromatic term) and transmission dispersions. The overall single photon resolution is estimated to be about 10 mrad.

8.3.1. Cherenkov Photon Detection Efficiency

Figure 53 shows the contribution of various optical and electronic components of the DIRC to the Cherenkov photon detection efficiency as a function of wavelength. The data points pertain to a particle entering the center of the bar at 90°. A typical design goal for the photon transport in the bar was that no single component should contribute more than 10–20% loss of detection efficiency. Satisfying this criterion required an extremely high internal reflection coefficient of the bar surfaces (greater than 0.9992 per bounce), so that about 80% of the light is maintained after multiple bounces along the bars (365 bounces in the example of Figure 53). The ultraviolet cut-off is at ~ 300 nm, determined by the epoxy (Epotek 301-2 [63]) used to glue the fused silica bars together. The dominant contributor to the overall detection efficiency is the quantum efficiency of the PMT. Taking into account additional wavelength independent factors, such as the PMT packing fraction and the geometrical efficiency for trapping Cherenkov photons in the fused silica bars via total internal reflection, the expected number of photoelectrons (N_{pe}) is ~ 28 for a $\beta = 1$ particle entering normal to the surface at the center of a bar, and increases by over a factor of two in the forward and backward directions.

8.3.2. DIRC Water System

The DIRC water system is designed to maintain good transparency at wavelengths as small as 300 nm. One way to achieve this is to use ultrapure, de-ionized water, close to the theoretical limit of 18 MΩcm resistivity. In addition, the water must be de-gassed and the entire system kept free of bacteria. Purified water is aggressive in attacking many materials, and those in contact with the water were selected based on known compatability with purified water. To maintain the necessary level of water quality, most plumbing components are made of stainless steel or polyvinylidene fluoride.

The system contains an input line with six mechanical filters (three 10 μm, two 5 μm, and one 1 μm), a reverse osmosis unit, de-ionization

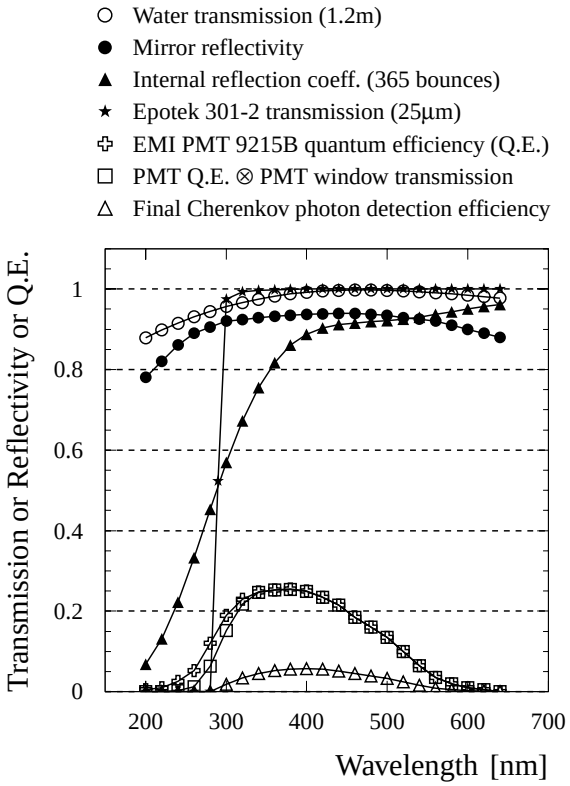

Figure 53. Transmission, reflectivity and quantum efficiency for various components of the DIRC as a function of wavelength for a $\beta = 1$ particle at normal incidence to the center of a bar [64].

beds, a Teflon microtube de-gasser and various pumps and valves. To prevent bacteria growth, it is equipped with a UV lamp (254 nm wavelength) and filters (two 1 μm, two 0.2 μm, and charcoal filters). Sampling ports are provided to check the water quality and to monitor resistivity, pH-value, temperature, and flow. A gravity feed return system prevents overpressure. The entire standoff box water volume can be recirculated up to four times a day.

The operating experience with the water system so far has been very good. The water volume is exchanged every ten hours and the resistivity of the water is typically 18 MΩcm in the supply line and 8–10 MΩcm in the return line at a temperature of about 23–26°C. The pH-value is about 6.5 and 6.6-6.7 in the supply and return water, respectively. The water transparency is routinely measured using lasers of three different wavelengths. The transmission is better than 92% per meter at 266 nm and exceeds 98% per meter at 325 nm and 442 nm.

Potential leaks from the water seals between the bar boxes and the standoff box are detected by a water leak detection system of 20 custom water sensors in and about the bar box slots. Two commercial ultrasonic flow sensors are used to monitor water flow in two (normally dry) drain lines in addition to the 12 humidity sensors on a nitrogen gas output line from each bar box (see below). Should water be detected, a valve in a 100 mm diameter drain line is opened, and the entire system is drained in about 12 minutes.

All elements inside the standoff box (PMT, plastic PMT housing, gaskets, light catchers) were tested at normal and elevated temperatures to withstand the highly corrosive action of ultrapure water and to prevent its pollution. For instance, rhodium-plated mirrors on ULTEM support had to be used for the light catchers [59].

8.3.3. DIRC Gas System

Nitrogen gas from liquid nitrogen boil-off is used to prevent moisture from condensing on the bars, and used also to detect water leaks. The gas flows through each bar box at the rate of 100–200 cm^3/min, and is monitored for humidity to ensure that the water seal around the bar box remains tight. The gas is filtered through a molecular sieve and three mechanical filters to remove particulates (7 μm, 0.5 μm, and 0.01 μm). Dew points of the gas returned from the bar boxes are about -40°C. Approximately one third of the input nitrogen gas leaks from the bar boxes and keeps the bar box slots in the mechanical support structure free of condensation.

8.4. Electronics

8.4.1. DIRC PMT Electronics

The DIRC PMT base contains a single printed circuit board, equipped with surface mounted components. The operating high voltage (HV) of the PMTs is $\sim$ 1.14 kV, with a range between

0.9 and 1.3 kV. Groups of 16 tubes are selected for uniformity of gain to allow their operation at a common HV provided from a single distribution board.

The HV is provided by a CAEN SY-527 high voltage distribution system. Each of the 12 sectors receives HV through 56 high voltage channels, distributed through a single cable bundle. Each voltage can be set between 0 and 1.6 kV.

8.4.2. DIRC Front-End Electronics

The DIRC front-end electronics (FEE) is designed to measure the arrival time of each Cherenkov photon detected by the PMT array [65] to an accuracy that is limited by the intrinsic 1.5 ns transit time spread of the PMTs. The design contains a pipeline to deal with the L1 trigger latency of 12μ s, and can handle random background rates of up to 200 kHz/PMT with zero dead time. In addition, the pulse height spectra can be measured to ensure that the PMTs operate on the HV plateau. However, because the ADC information is not needed to reconstruct events, 64 PMTs are multiplexed onto a single ADC for monitoring and calibration.

The DIRC FEE is mounted on the outside of the standoff box and is highly integrated in order to minimize cable lengths and to retain the required single photoelectron sensitivity. Each of the 168 DIRC *Front-end Boards* (DFBs) processes 64 PMT inputs, containing eight custom analog chips along with their associated level translators, four custom-made TDC ICs, one 8-bit flash ADC (FADC), two digitally controlled calibration signal generators, multi-event buffers, and test hardware.

The PMT signals are amplified, and pulse-shaped by an eight-channel analog IC [66]. A digital pulse timed with the peak of the input pulse is output by a zero-crossing discriminator, as well as a pulse shaped by a CR-RC filter with 80 ns peaking time, which was chosen to allow for the ADC multiplexing. The multiplexer selects the channel to be digitized by the FADC for calibration.

The TDC IC [67] is a 16-channel TDC with 0.5 ns binning, input buffering, and selective readout of the data in time with the trigger. To cope with the L1 maximum trigger latency of 12 μs and jitter of 1 μs, the selective readout process extracts data in time with the trigger within a programmable time window. The acceptance window width is programmable between 64 ns and 2 μs and is typically set at 600 ns. The twelve DIRC Crate Controllers (DCCs) that form the interface to the VME front-end crates are connected to six ROMs via 1.2 Gbit/s optical fibers.

8.4.3. DAQ Feature Extraction

Raw data from the DFBs are processed in the ROMs by a feature extraction algorithm before being transmitted to the segment and event builder. This software algorithm reduces the data volume by roughly 50% under typical background conditions. DFB data that contain errors are flagged and discarded. The only data errors seen to date have been traced to damaged DFBs that were replaced immediately. Because the dataflow system can reliably transmit at most 32 kBytes/crate, the feature extraction must sometimes truncate data to limit the event size. Event data are replaced with a per-DFB occupancy summary when a ROM's hit occupancy exceeds 56%, which occurs about once in 10^4 events. An appropriate flag is inserted into the feature extraction output whenever truncation or deletion occurs. Errors, truncation, and feature extraction performance are continuously monitored online, and exceptions are either immediately corrected or logged for future action.

8.4.4. DIRC Calibration

The DIRC uses two independent approaches for a calibration of the unknown PMT time response and the delays introduced by the FEE and the fast control system. The first is a conventional pulser calibration. The second uses reconstructed tracks from collision data.

The pulser calibration is performed online using a light pulser system which generates precisely timed 1 ns duration light pulses from twelve, blue LEDs, one per sector. The LEDs are triggered by the global fast control calibration strobe command sent to the DCCs. The DCC triggers an individual LED for each sector upon receipt of calibration strobe. Pulses in adjacent sectors are

staggered by 50 ns to prevent light crosstalk between sectors. The pulser is run at roughly 2 kHz for the time delay calibration. The LED light is transmitted through approximately 47 m-long optical fibers to diffusers mounted on the inner surface of the standoff box wall opposite the PMTs. This light produces about 10% photoelectron occupancy nearly uniformly throughout the standoff box.

Histograms of TDC times for each PMT are accumulated in parallel in the ROMs, and then fit to an asymmetric peak function. About 65,000 light pulses are used to determine the mean time delay of each of the PMTs in the standoff box to a statistical accuracy of better than 0.1 ns. The LED pulser is also used to monitor the phototube gains using the ADC readout. As with the TDC calibration, histograms and fits of the ADC spectrum are accumulated and fit in the ROM. A calibration run including both TDC and ADC information for all PMTs requires a few minutes, and is run once per day. Daily calibrations not only verify the time delays, but allow the detection of hardware failures.

The data stream calibration uses reconstructed tracks from the collision data. For calibration of the global time delay, the observed, uncalibrated times minus the expected arrival times, Δt_γ, are collected during the online prompt reconstruction processing. To calculate individual channel calibrations, Δt_γ values for each DIRC channel are accumulated until statistics equivalent to 100,000 tracks are collected. The distribution for each channel is fit to extract the global time offset calibration.

The data stream and online pulser calibrations of the electronic delays, and of the PMT time response and gain yield fully consistent results, although the data stream results in 15% better timing resolution than the pulser calibration. The time delay values per channel are typically stable to an *rms* of less than 0.1 ns over more than one year of daily calibrations.

8.4.5. DIRC Environmental Monitoring System

The DIRC environmental monitoring system is divided into three parts, corresponding to three separate tasks. The first deals with the control and monitoring of the HV system for the PMTs. The second is devoted to monitoring low voltages related to the FEE. The third controls a variety of other detector parameter settings. An interlock system, based on a standard VME module (SIAM), is provided. For the purposes of the DIRC, three dedicated VME CPUs run the application code. The communication between the HV mainframes and the monitoring crate is achieved by a CAENET controller (V288). The HV monitor task controls the step sizes for ramping the HV up or down, as well as the communication of alarm conditions, and the values and limits for the HV and current of each channel.

The purpose of FEE monitoring is to control and monitor parameters related to the FEE. For each DIRC sector, a custom multipurpose board, the DCC, equipped with a microcontroller [68] incorporating the appropriate communication protocol (CANbus), is situated in the same crate as the DFB. All monitoring and control tasks are implemented on this card. The parameters monitored are the low voltages for the DFBs and DCCs, the status of the optical link (Finisar), the temperature on supply boards, and the VME crate status.

The third part of the monitoring system is based on a custom ADC VME board (VSAM), used to monitor various type of sensors: magnetic field sensors, an ensemble of 12 beam monitoring scalers, 16 CsI radiation monitors, the water level in the standoff box as well as its pH-value, resistivity, and temperature.

8.5. Operational Issues

The DIRC was successfully commissioned and attained performance close to that expected from Monte Carlo simulation. The DIRC has been robust and stable, and, indeed, serves also as a background detector for PEP-II tuning. Figure 54 shows a typical di-muon event ($e^+e^- \to \mu^+\mu^-$). In addition to the signals caused by the Cherenkov light from the two tracks, about 500 background signals can be seen in the readout window of $\pm$300 ns. This background is dominated by low energy photons from the PEP-II machine hitting the standoff box. Some care in

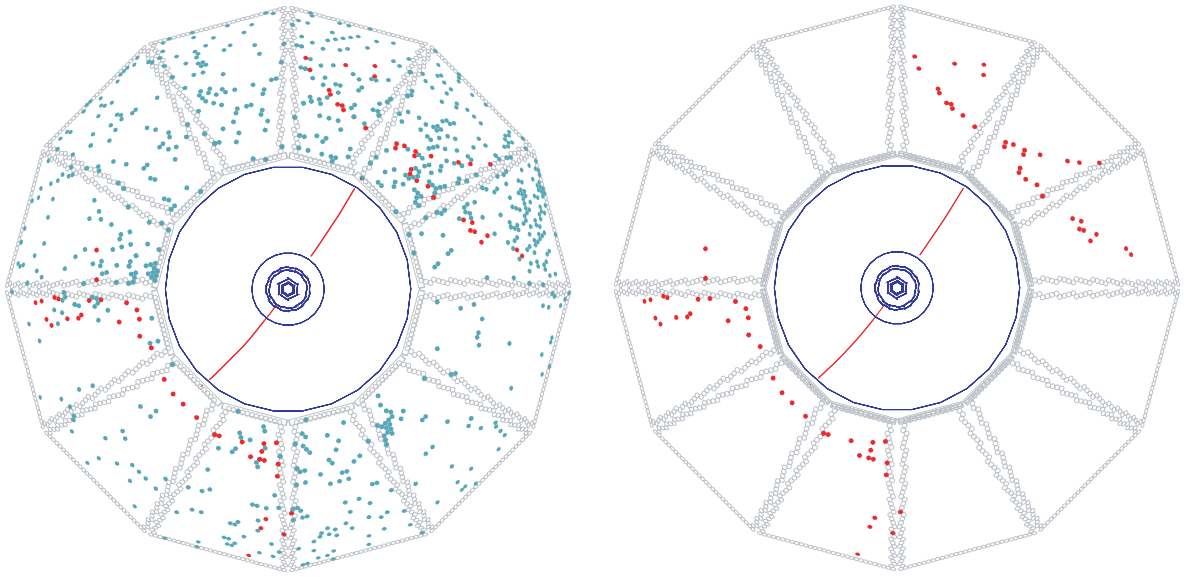

Figure 54. Display of an $e^+e^- \to \mu^+\mu^-$ event reconstructed in *BABAR* with two different time cuts. On the left, all DIRC PMTs with signals within the ±300 ns trigger window are shown. On the right, only those PMTs with signals within 8 ns of the expected Cherenkov photon arrival time are displayed.

machine tuning is required to stay under a noise limit of about 200 kHz/tube imposed by limited DAQ throughput. Lead shielding has been installed around the beam line components just outside the backward endcap, and has substantially reduced this background.

After about two years of running, approximately 99.7% of PMTs and electronic channels are operating with nominal performance.

Some deterioration of the PMT front glass windows (made of B53 Borosilicate glass) that are immersed in the ultra-pure water of the standoff box has been observed. For most of the tubes, the observable effect is typically a slight cloudiness, but for about 50 tubes, it is much more pronounced. Extensive R&D has demonstrated that the effect is associated with a loss of sodium and boron from the surface of the glass [69]. For most tubes, the leaching rate is a few microns per year, and is expected to be acceptable for the full projected ten year lifetime of the experiment. However, for the $\sim$ 50 tubes, the incorrect glass was used by the manufacturer. That glass does not contain zinc, making it much more susceptible to rapid leaching. This leaching may eventually lead to either a loss of performance, or some risk of mechanical failure of the face plates for these tubes. Direct measurements of the number of Cherenkov photons observed in di-muon events as a function of time suggest that the total loss of photons from all sources is less than 2%/year.

8.6. Data Analysis and Performance

Figure 54 shows the pattern of Cherenkov photons in a di-muon event, before and after reconstruction. The time distribution of real Cherenkov photons from a single event is of order $\sim$ 50 ns wide, and during normal data-taking they are accompanied by hundreds of random photons in a flat background within the trigger acceptance window. Given a track pointing at a particular fused silica bar and a candidate signal in a PMT within the optical phase space of that bar, the Cherenkov angle is determined up to a 16-fold ambiguity: top or bottom, left or right, forward or backward, and wedge or no-wedge reflections. The goal of the reconstruction program is to associate the correct track with the candidate PMT signal, with the requirement that the transit time of the photon from its creation in the bar to its

detection at the PMT be consistent with the measurement error of ~ 1.5 ns.

8.6.1. Reconstruction

An unbinned maximum likelihood formalism is used to incorporate all information provided by the space and time measurements from the DIRC.

The emission angle and the arrival time of the Cherenkov photons are reconstructed from the observed space-time coordinates of the PMT signals, transformed into the Cherenkov coordinate system (θ_c, ϕ_c, and δt) as follows: The known spatial position of the bar through which the track passed and the PMTs whose signal times lie within the readout window of ± 300 ns from the trigger are used to calculate the three-dimensional vector pointing from the center of the bar end to the center of each tube. This vector is then extrapolated into the radiator bar (using Snell's law). This procedure defines, up to the 16-fold ambiguity described above, the angles θ_c and ϕ_c of a photon.

The DIRC time measurement represents the third dimension of the photomultiplier hit reconstruction. The timing resolution is not competitive with the position information for Cherenkov angle reconstruction, but timing information is used to suppress background hits from the beam induced background and, more importantly, exclude other tracks in the same event as the source of the photon. Timing information is also used to resolve the forward-backward and wedge ambiguities in the hit-to-track association.

The relevant observable to distinguish between signal and background photons is the difference between the measured and expected photon arrival time, Δt_γ. It is calculated for each photon using the track time-of-flight (assuming it to be a charged pion), the measured time of the candidate signal in the PMT and the photon propagation time within the bar and the water filled standoff box. The time information and the requirement of using only physically possible photon propagation paths reduce the number of ambiguities from 16 to typically 3. Applying the time information also substantially improves the correct matching of photons with tracks and reduces the number of accelerator induced background signals by approximately a factor 40, as illustrated in Figure 54.

The reconstruction routine currently provides a likelihood value for each of the five stable particle types (e,μ,π,K,p) if the track passes through the active volume of the DIRC. These likelihoods are calculated in an iterative process by maximizing the likelihood value for the entire event while testing different hypotheses for each track. If enough photons are found, a fit of θ_c and the number of observed signal and background photons are calculated for each track.

8.6.2. Results

The parameters of expected DIRC performance were derived from extensive studies with a variety of prototypes, culminating with a full-size prototype in a beam at CERN [70]. The test beam results were well-described by Monte Carlo simulations of the detector. The performance of the full detector is close to expectations, and additional offline work, particularly on geometrical alignment, is expected to lead to further improvements.

In the absence of correlated systematic errors, the resolution ($\sigma_{C,\mathrm{track}}$) on the track Cherenkov angle should scale as

$$\sigma_{C,\mathrm{track}} = \frac{\sigma_{C,\gamma}}{\sqrt{N_{pe}}}, \tag{5}$$

where $\sigma_{C,\gamma}$ is the single photon Cherenkov angle resolution, and N_{pe} is the number of photons detected. Figure 55(a) shows the single photon angular resolution obtained from di-muon events. There is a broad background of less than 10% relative height under the peak, that originates mostly from track-associated sources, such as δ rays, and combinatorial background. The width of the peak translates to a resolution of about 10.2 mrad, in good agreement with the expected value. The measured time resolution (see Figure 55(b)) is 1.7 ns, close to the intrinsic 1.5 ns transit time spread of the PMTs.

The number of photoelectrons shown in Figure 56 varies between 20 for small polar angles at the center of the barrel and 65 at large polar angles. This variation is well reproduced by Monte Carlo simulation, and can be understood from the

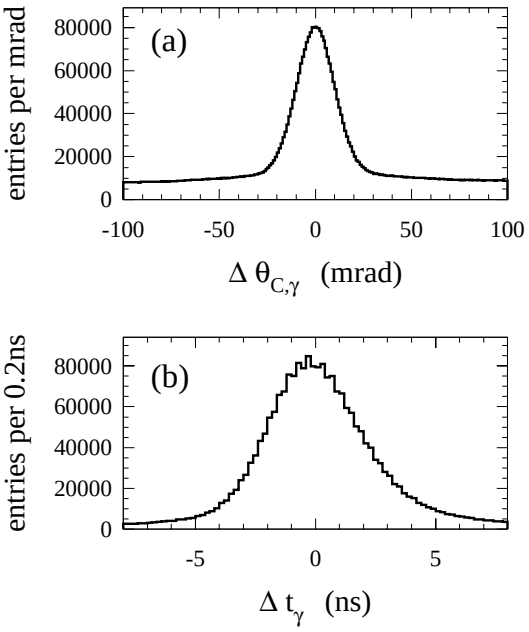

Figure 55. The difference between (a) the measured and expected Cherenkov angle for single photons, $\Delta\theta_{c,\gamma}$, and (b) the measured and expected photon arrival time, for single muons in $\mu^+\mu^-$ events.

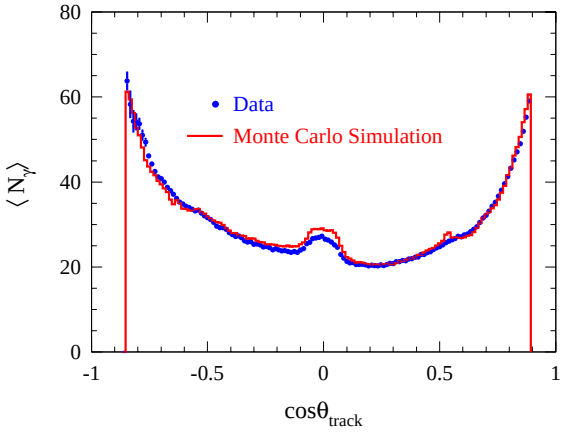

Figure 56. Number of detected photons versus track polar angle for reconstructed tracks in di-muon events compared to Monte Carlos simulation. The mean number of photons in the simulation has been tuned to match the data.

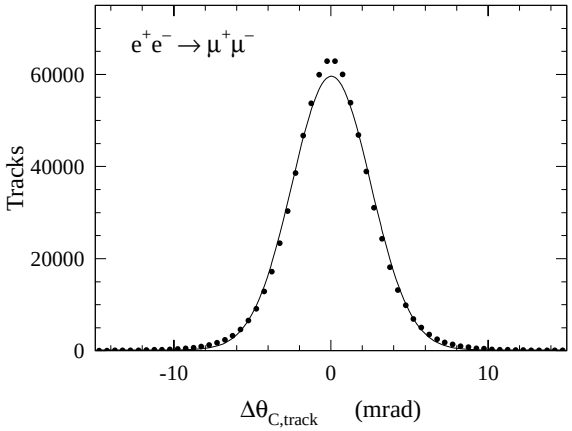

Figure 57. The difference between the measured and expected Cherenkov angle, $\Delta\theta_{c,track}$, for single muons in $\mu^+\mu^-$ events. The curve represents a Gaussian distribution fit to the data with a width of 2.5 mrad.

geometry of the DIRC. The number of Cherenkov photons varies with the pathlength of the track in the radiator, it is smallest at perpendicular incidence at the center and increases towards the ends of the bars. In addition, the fraction of photons trapped by total internal reflection rises with larger values of $|\cos\theta_{\rm track}|$. This increase in the number of photons for forward going tracks is a good match to the increase in momentum and thus benefits the DIRC performance.

With the present alignment, the track Cherenkov angle resolution for di-muon events is shown in Figure 57. The width of the fitted Gaussian distribution is 2.5 mrad compared to the design goal of 2.2 mrad. From the measured single track resolution versus momentum in di-muon events and the difference between the expected Cherenkov angles of charged pions and kaons, the pion-kaon separation power of the DIRC can be inferred. As shown in Figure 58, the expected separation between kaons and pions at 3 GeV/c is about 4.2σ, within 15% of the design goal.

Figure 59 shows an example of the use of the DIRC for particle identification. The $K\pi$ invariant mass spectra are shown with and without the use of the DIRC for kaon identification. The peak corresponds to the decay of the D^0 particle.

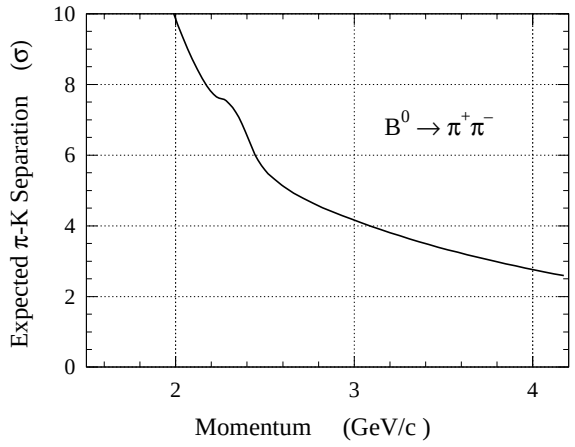

Figure 58. Expected π-K separation in $B^0 \to \pi^+\pi^-$ events versus track momentum inferred from the measured Cherenkov angle resolution and number of Cherenkov photons per track in di-muon events.

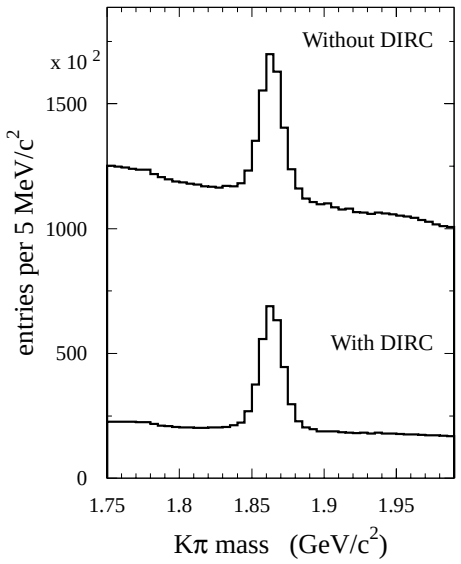

Figure 59. Invariant Kπ inclusive mass spectrum with and without the use of the DIRC for kaon identification. The mass peak corresponds to the decay of the D^0 particle.

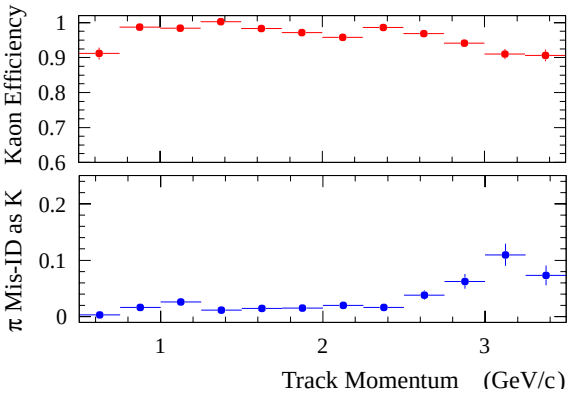

Figure 60. Efficiency and misidentification probability for the selection of charged kaons as a function of track momentum, determined using $D^0 \to K^-\pi^+$ decays selected kinematically from inclusive D^* production.

The efficiency for correctly identifying a charged kaon that traverses a radiator bar and the probability to wrongly identify a pion as a kaon are determined using $D^0 \to K^-\pi^+$ decays selected kinematically from inclusive D^* production and are shown as a function of the track momentum in Figure 60 for a particular choice of particle selection criteria. The mean kaon selection efficiency and pion misidentification are $96.2 \pm 0.2\%$ (stat.) and $2.1 \pm 0.1\%$ (stat.), respectively.

8.7. Summary

The DIRC is a novel ring-imaging Cherenkov detector that is well-matched to the hadronic PID requirements of *BABAR*. The DIRC has been robust and stable and, two years after installation, about 99.7% of all PMTs and electronic channels are operating with nominal performance. Additional shielding in the standoff box tunnel region should reduce the sensitivity to beam-induced backgrounds, as should faster FEE, both installed during the winter 2000-2001 shutdown. At luminosities around $1 \times 10^{34}\,\mathrm{cm}^{-2}\mathrm{s}^{-1}$, the TDC IC will have to be replaced with a faster version and deeper buffering. The design process for this is underway.

The detector performance achieved is rather

close to that predicted by the Monte Carlo simulations. Alignment and further code developments are expected to further improve performance.